Journal of Naval Architecture and Marine Engineering
June, 2024
http://dx.doi.org/10.3329/jname.v21i1.70846 *http://www.banglajol.info*

ANALYTICAL SOLUTIONS OF POISEUILLE FLOW OF SECOND-GRADE FLUID

Venkat Rao Kanuri[1,2*], K.V.Chandra Sekhar[3], P.S.Brahmanandam[4], J.V.Ramanaiah[5]
[1]Research Scholar, Department of Mathematics, K L University, Vaddeswaram - 522302.
[2]Department of Mathematics, SRKR Engineering College(A), Bhimavaram-534204, *k.ravi.msc@gmail.com
[3]Department of Mathematics, K L University, Vaddeswaram- 522302, chandu_fed@kluniversity.in
[4]Department of Basic Sciences, Shri Vishnu Engineering College for Women(A), Bhimavaram-534202, anand1576@gmail.com
[5]Department of Mathematics, Aditya College of Engineering and Technology, Surampalem 533437, venkataramanaiah_bse@acoe.edu.in

Abstract:

Poiseuille flows are considered as flows of Newtonian fluids through stationary pipes, with applications ranging from the pharmaceutical industries to manufacturing companies. These flows have been extensively studied in several works of literature due to their relevance in many spheres of life. However, the Poiseuille flow for non-Newtonian flows has not gained much attention, even though most fluids are non-Newtonian. Based on this, this study investigates the Poiseuille flow of the second-grade fluid. Second-grade fluids are viscoelastic non-Newtonian fluids that exhibit both shear-thinning and shear-thickening with applications found in several industrial applications such as pharmaceutical, cosmetics and polymer processing. The Poiseuille flow of second-grade fluid is formulated from the underlying Navier-Stokes' equations and the general assumptions of Poiseuille flow are invoked to reduce the equations to the regular ordinary differential equations. An analytical solution for the flow problem is sought using the method of separation of variables and the results are graphed to show the response of velocity and flow rate to the parameters of the flow. The outcomes show that velocity distribution reduces as the pipe radius increases and second-grade fluid has lower velocity than the Newtonian fluid.

Keywords: Poiseuille flow, Couette flow, second-grade fluid, non-Newtonian fluid, Navier-Stokes' equations.

NOMENCLATURE

$\vec{V}$	velocity vector
p	pressure

Greek symbols

μ	dynamic viscosity
σ	stress sensor

1. Introduction

Non-Newtonian fluids are fluids whose shear strain responds nonlinearly to the shear stress. Examples of non-Newtonian fluids include the Casson fluid (Reddy and Reddy, 2022; Oke et al., 2020), Williamson fluid (Divya et al., 2023), Carreau fluid (Murthy and Reddy, 2023), Eyring-Powell fluid (Oke et al., 2023), modified Eyring-Powell fluid (see Oke, 2021; Oke 2022) and second-grade fluid (Krishna, 2021). Second-grade fluids are non-Newtonian fluids of the viscoelastic type, exhibiting a second-order relationship between the shear stress and shear strain. They can shear-thin or shear-thicken depending on the particular choice of second-grade fluid. The behaviour of the second-grade fluids depends both on the current state, as well as the past deformation history. Examples of second-grade fluid include ketchup and blood with applications found in several industrial applications such as pharmaceutical, cosmetics and polymer processing. Krishna (2021) studied the Hall slip on unsteady MHD flow of second-grade and the results include some novel applications of second-grade fluid in aerospace science. Yavuz (2022) extended the partial differential equations to the fractional order equations. The Laplace transform was used to solve the equations and the results showed that velocity profile reduces with increasing Prandtl number. Other studies include Oke et al. (2021), Juma et al. (2022), Oke (2022b), Vyakaranam (2022), Oke (2022c), Reni et al. (2023).

Flows in diverse geometries of pipes and channels are ubiquitous in applications and are usually classed as Couette or Poiseuille flow depending on the relative motion of the channel walls (Kumar et al., 2018a; Kumar et al., 2018b;

1813-8535 (Print), 2070-8998 (Online) © 2024 ANAME Publication. All rights reserved. Received on: Jan., 2024

Kumar et al., 2019a; Kumar et al., 2019b; Kumar et al., 2020). Poiseuille flow is a flow driven by pressure differential whereas Couette flow concerns flow between relatively moving parallel plates (Coles, 1965). Poiseuille flow is characterized by a flow of non-overlapping layers (that is, laminar flow) of viscous fluid sustained by the pressure variation (Gee & Gracie, 2022). The velocity profile in a Poiseuille flow is a symmetrical parabola with a maximum point at the midpoint but no flow on the wall (Wu et al., 2023). Poiseuille flow is essential for the design and development of microfluidic devices because the velocity gradient in this profile improves material transport. Other real-world uses for the Poiseuille flow can be found in many industrial processes and blood flow through capillaries. Poiseuille flow can be used to mimic the flow of blood in capillaries. It can be used to simulate industrial processes such as fluid transport in pipelines, heat exchanger systems, and chemical reactors, which have applications in the petroleum industry and other large-scale businesses (Sulaimon, 2023). The implementation of Poiseuille flow in sophisticated medical diagnostics, medication delivery, and microscale chemical analysis is easily traced to the elegance in obtaining the solution of such flow.

In this study, the Poiseuille flow of second-grade fluid is investigated within a pipe. Most works of literature have extensively considered Poiseuille flow for Newtonian fluids in different geometries, but none has specifically identified a non-Newtonian fluid to consider the analytical solution of such Poiseuille flow. The selected geometry for our study, a cylindrical pipe, reflects its widespread application in various engineering and biomedical fields. Though simple, the representative nature allows for a focused investigation of the Poiseuille flow of second-grade fluid. Inspired by its importance in fluid transport systems and microfluidic devices, we chose this geometry to elucidate the behaviour of non-Newtonian fluids in a practical setting. This study provides answers to the following research questions:

(i) What is the effect of viscosity on flow velocity and flow rate of a Poiseuille second-grade fluid flow?

(ii) What is the effect of second-grade fluid parameters on flow velocity and flow rate of a Poiseuille second-grade fluid flow?

2. Flow Description and Model Development

Figure 1 shows a prototype of the fluid flow between two plates separated by a diameter of $2h$. The flow region is symmetrical about the origin $y = 0$. An incompressible steady second-grade fluid flows between the stationary plates and the flow is considered after it is fully well-developed.

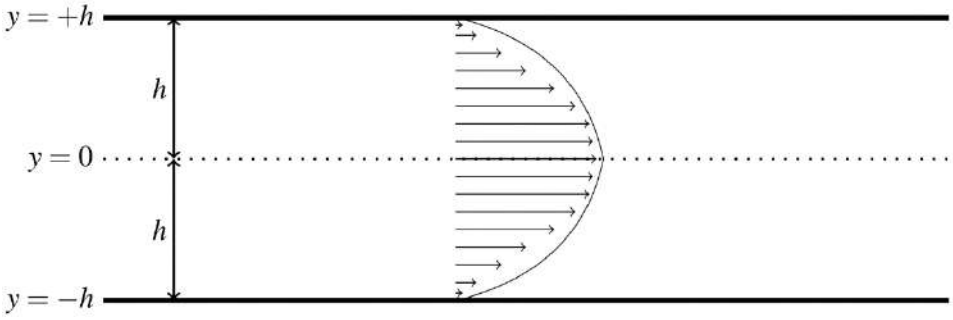

Figure 1: Flow configuration

The continuity equation, according to Oke et al. (2020) and Sitamahalakshmi et al. (2023) governing the steady flow of the second-grade fluid is

$$\nabla \cdot \vec{\boldsymbol{V}} = 0 \tag{2.1}$$

and $\vec{\boldsymbol{V}}$ is the velocity vector defined as $\vec{\boldsymbol{V}} = (u_1, u_2, u_3)$ and ∇ is the gradient operator in 3-dimension defined as

$$\nabla = \frac{\partial}{\partial x_1} + \frac{\partial}{\partial x_2} + \frac{\partial}{\partial x_3}.$$

In general, the continuity equation can be rewritten as

$$\frac{\partial u_1}{\partial x_1} + \frac{\partial u_2}{\partial x_2} + \frac{\partial u_3}{\partial x_3} = 0 \tag{2.2}$$

Following the work of Kọríkọ (2020), the law of conservation of momentum is

$$\rho\left(\frac{\partial \vec{\boldsymbol{V}}}{\partial t} + (\vec{\boldsymbol{V}} \cdot \nabla)\vec{\boldsymbol{V}}\right) = \nabla \cdot \boldsymbol{\sigma} + \rho b \tag{2.3}$$

where the stress tensor is represented as $\boldsymbol{\sigma}$ and b stands for the possible body forces. Since the flow is steady, then the velocity is independent of time and the equation (2.3) becomes

$$\rho(\vec{\boldsymbol{V}} \cdot \nabla)\vec{\boldsymbol{V}} = \nabla \cdot \boldsymbol{\sigma} + \rho b. \tag{2.4}$$

According to Ayub and Zaman (2010), the stress tensor for the second-grade fluid has a quadratic relationship of the form

$$\boldsymbol{\sigma} = -p\boldsymbol{I} + \mu\boldsymbol{A}_1 + \alpha_1\boldsymbol{A}_2 + \alpha_2\boldsymbol{A}_1^2.$$

The terms in the equation are the identity tensor $\boldsymbol{I}$, pressure p, dynamic viscosity $\mu \geq 0$, fluid constants α_1, α_2 and the Rivillin Ericksen tensors $\boldsymbol{A}_1, \boldsymbol{A}_2$ whose representations are given in Anderson (1992) and Beard (1964) as

$$\boldsymbol{A}_1 = \nabla\boldsymbol{V} + (\nabla\boldsymbol{V})^T,$$

$$\boldsymbol{A}_2 = \frac{\partial \boldsymbol{A}_1}{\partial t} + (\boldsymbol{V} \cdot \nabla)\boldsymbol{A}_1 + \boldsymbol{A}_1(\nabla\boldsymbol{V}) + (\nabla\boldsymbol{V})^T\boldsymbol{A}_1.$$

$$= (\boldsymbol{V} \cdot \nabla)\boldsymbol{A}_1 + \boldsymbol{A}_1(\nabla\boldsymbol{V}) + (\nabla\boldsymbol{V})^T\boldsymbol{A}_1, \ \ since \quad \frac{\partial \boldsymbol{A}_1}{\partial t} = 0 \ \ for\ steady\ flow.$$

$$= (\boldsymbol{V} \cdot \nabla)\boldsymbol{A}_1 + \boldsymbol{A}_1(\nabla\boldsymbol{V}) + \left(\boldsymbol{A}_1^T(\nabla\boldsymbol{V})\right)^T,$$

where $\nabla\boldsymbol{V} = \left(\frac{\partial u_i}{\partial x_j}\right)$, , $i, j = 1,2,3.$

Since $u_2 = u_3 = 0$ and there is no flow in the z-direction, then

$$\nabla\boldsymbol{V} = \begin{pmatrix} \frac{\partial u_1}{\partial x_1} & \frac{\partial u_1}{\partial x_2} & 0 \\ 0 & 0 & 0 \\ 0 & 0 & 0 \end{pmatrix} \Rightarrow (\nabla\boldsymbol{V})^T = \begin{pmatrix} \frac{\partial u_1}{\partial x_1} & 0 & 0 \\ \frac{\partial u_1}{\partial x_2} & 0 & 0 \\ 0 & 0 & 0 \end{pmatrix}$$

and

$$\boldsymbol{A}_1 = \nabla\boldsymbol{V} + (\nabla\boldsymbol{V})^T = \begin{pmatrix} 2\frac{\partial u_1}{\partial x_1} & \frac{\partial u_1}{\partial x_2} & 0 \\ \frac{\partial u_1}{\partial x_2} & 0 & 0 \\ 0 & 0 & 0 \end{pmatrix}$$

$$\boldsymbol{A}_1^2 = \begin{pmatrix} 2\frac{\partial u_1}{\partial x_1} & \frac{\partial u_1}{\partial x_2} & 0 \\ \frac{\partial u_1}{\partial x_2} & 0 & 0 \\ 0 & 0 & 0 \end{pmatrix}\begin{pmatrix} 2\frac{\partial u_1}{\partial x_1} & \frac{\partial u_1}{\partial x_2} & 0 \\ \frac{\partial u_1}{\partial x_2} & 0 & 0 \\ 0 & 0 & 0 \end{pmatrix} = \begin{pmatrix} 4\left(\frac{\partial u_1}{\partial x_1}\right)^2 + \left(\frac{\partial u_1}{\partial x_2}\right)^2 & 2\frac{\partial u_1}{\partial x_1}\frac{\partial u_1}{\partial x_2} & 0 \\ 2\frac{\partial u_1}{\partial x_1}\frac{\partial u_1}{\partial x_2} & \left(\frac{\partial u_1}{\partial x_2}\right)^2 & 0 \\ 0 & 0 & 0 \end{pmatrix}.$$

By noting that $\boldsymbol{A}_1$ is symmetric then,

$$\boldsymbol{A}_2 = (\boldsymbol{V} \cdot \nabla)\boldsymbol{A}_1 + \boldsymbol{A}_1(\nabla\boldsymbol{V}) + \left(\boldsymbol{A}_1(\nabla\boldsymbol{V})\right)^T. \tag{2.5}$$

Now,

$$\boldsymbol{A}_1(\nabla\boldsymbol{V}) = \begin{pmatrix} 2\frac{\partial u_1}{\partial x_1} & \frac{\partial u_1}{\partial x_2} & 0 \\ \frac{\partial u_1}{\partial x_2} & 0 & 0 \\ 0 & 0 & 0 \end{pmatrix}\begin{pmatrix} \frac{\partial u_1}{\partial x_1} & \frac{\partial u_1}{\partial x_2} & 0 \\ 0 & 0 & 0 \\ 0 & 0 & 0 \end{pmatrix} = \begin{pmatrix} 2\left(\frac{\partial u_1}{\partial x_1}\right)^2 & 2\frac{\partial u_1}{\partial x_1}\frac{\partial u_1}{\partial x_2} & 0 \\ \frac{\partial u_1}{\partial x_1}\frac{\partial u_1}{\partial x_2} & \left(\frac{\partial u_1}{\partial x_2}\right)^2 & 0 \\ 0 & 0 & 0 \end{pmatrix},$$

$$\left(\boldsymbol{A}_1(\nabla \boldsymbol{V})\right)^T = \begin{pmatrix} 2\left(\frac{\partial u_1}{\partial x_1}\right)^2 & \frac{\partial u_1}{\partial x_1}\frac{\partial u_1}{\partial x_2} & 0 \\ 2\frac{\partial u_1}{\partial x_1}\frac{\partial u_1}{\partial x_2} & \left(\frac{\partial u_1}{\partial x_2}\right)^2 & 0 \\ 0 & 0 & 0 \end{pmatrix}.$$

and

$$\boldsymbol{A}_1(\nabla \boldsymbol{V}) + \left(\boldsymbol{A}_1(\nabla \boldsymbol{V})\right)^T = \begin{pmatrix} 4\left(\frac{\partial u_1}{\partial x_1}\right)^2 & 3\frac{\partial u_1}{\partial x_1}\frac{\partial u_1}{\partial x_2} & 0 \\ 3\frac{\partial u_1}{\partial x_1}\frac{\partial u_1}{\partial x_2} & 2\left(\frac{\partial u_1}{\partial x_2}\right)^2 & 0 \\ 0 & 0 & 0 \end{pmatrix}.$$

Next,

$$(\boldsymbol{V}\cdot\nabla)\boldsymbol{A}_1 = \left(u_1\frac{\partial}{\partial x_1} + u_2\frac{\partial}{\partial x_2} + u_3\frac{\partial}{\partial x_3}\right)\begin{pmatrix} 2\frac{\partial u_1}{\partial x_1} & \frac{\partial u_1}{\partial x_2} & 0 \\ \frac{\partial u_1}{\partial x_2} & 0 & 0 \\ 0 & 0 & 0 \end{pmatrix}$$

$$= u_1\frac{\partial}{\partial x_1}\begin{pmatrix} 2\frac{\partial u_1}{\partial x_1} & \frac{\partial u_1}{\partial x_2} & 0 \\ \frac{\partial u_1}{\partial x_2} & 0 & 0 \\ 0 & 0 & 0 \end{pmatrix} = \begin{pmatrix} 2u_1\frac{\partial^2 u_1}{\partial x_1^2} & u_1\frac{\partial^2 u_1}{\partial x_1 \partial x_2} & 0 \\ u_1\frac{\partial^2 u_1}{\partial x_1 \partial x_2} & 0 & 0 \\ 0 & 0 & 0 \end{pmatrix}$$

and

$$\boldsymbol{A}_2 = \begin{pmatrix} 2u_1\frac{\partial^2 u_1}{\partial x_1^2} & u_1\frac{\partial^2 u_1}{\partial x_1 \partial x_2} & 0 \\ u_1\frac{\partial^2 u_1}{\partial x_1 \partial x_2} & 0 & 0 \\ 0 & 0 & 0 \end{pmatrix} + \begin{pmatrix} 4\left(\frac{\partial u_1}{\partial x_1}\right)^2 & 3\frac{\partial u_1}{\partial x_1}\frac{\partial u_1}{\partial x_2} & 0 \\ 3\frac{\partial u_1}{\partial x_1}\frac{\partial u_1}{\partial x_2} & 2\left(\frac{\partial u_1}{\partial x_2}\right)^2 & 0 \\ 0 & 0 & 0 \end{pmatrix}.$$

$$= \begin{pmatrix} 2u_1\frac{\partial^2 u_1}{\partial x_1^2} + 4\left(\frac{\partial u_1}{\partial x_1}\right)^2 & u_1\frac{\partial^2 u_1}{\partial x_1 \partial x_2} + 3\frac{\partial u_1}{\partial x_1}\frac{\partial u_1}{\partial x_2} & 0 \\ u_1\frac{\partial^2 u_1}{\partial x_1 \partial x_2} + 3\frac{\partial u_1}{\partial x_1}\frac{\partial u_1}{\partial x_2} & 2\left(\frac{\partial u_1}{\partial x_2}\right)^2 & 0 \\ 0 & 0 & 0 \end{pmatrix}.$$

The stress tensor is

$$\boldsymbol{\sigma} = \begin{pmatrix} \begin{bmatrix} -p + 2\mu\frac{\partial u_1}{\partial x_1} + 2\alpha_1 u_1\frac{\partial^2 u_1}{\partial x_1^2} + 4\alpha_1\left(\frac{\partial u_1}{\partial x_1}\right)^2 \\ +4\alpha_2\left(\frac{\partial u_1}{\partial x_1}\right)^2 + \alpha_2\left(\frac{\partial u_1}{\partial x_2}\right)^2 \end{bmatrix} & \begin{bmatrix} \mu\frac{\partial u_1}{\partial x_2} + \alpha_1 u_1\frac{\partial^2 u_1}{\partial x_1 \partial x_2} \\ +3\alpha_1\frac{\partial u_1}{\partial x_1}\frac{\partial u_1}{\partial x_2} + 2\alpha_2\frac{\partial u_1}{\partial x_1}\frac{\partial u_1}{\partial x_2} \end{bmatrix} & 0 \\ \mu\frac{\partial u_1}{\partial x_2} + \alpha_1 u_1\frac{\partial^2 u_1}{\partial x_1 \partial x_2} + 3\alpha_1\frac{\partial u_1}{\partial x_1}\frac{\partial u_1}{\partial x_2} + 2\alpha_2\frac{\partial u_1}{\partial x_1}\frac{\partial u_1}{\partial x_2} & -p + 2\alpha_1\left(\frac{\partial u_1}{\partial x_2}\right)^2 + \alpha_2\left(\frac{\partial u_1}{\partial x_2}\right)^2 & 0 \\ 0 & 0 & -p \end{pmatrix}.$$

Based on the assumption that the flow is considered when it is fully developed in the x-direction, then

$$u_2 = u_3 = 0. \tag{2.6}$$

It is therefore clear that

$$\frac{\partial u_2}{\partial x_2} = \frac{\partial u_3}{\partial x_3} = 0. \tag{2.7}$$

and the continuity equation (2.2) becomes

$$\frac{\partial u_1}{\partial x_1} + \frac{\partial u_2}{\partial x_2} + \frac{\partial u_3}{\partial x_3} = 0$$

$$\Rightarrow \frac{\partial u_1}{\partial x_1} = 0 \tag{2.8}$$

and

$$\boldsymbol{\sigma} = \begin{pmatrix} -p & \mu\dfrac{\partial u_1}{\partial x_2} & 0 \\ \mu\dfrac{\partial u_1}{\partial x_2} & -p + (2\alpha_1 + \alpha_2)\left(\dfrac{\partial u_1}{\partial x_2}\right)^2 & 0 \\ 0 & 0 & -p \end{pmatrix}.$$

The components of $\nabla \cdot \boldsymbol{\sigma}$ in the three directions are

$$\nabla \cdot \boldsymbol{\sigma}|_x = -\frac{\partial p}{\partial x_1} + \frac{\partial}{\partial x_2}\left(\mu\frac{\partial u_1}{\partial x_2}\right)$$

$$\nabla \cdot \boldsymbol{\sigma}|_y = -\frac{\partial p}{\partial x_2} + (2\alpha_1 + \alpha_2)\frac{\partial}{\partial x_2}\left(\frac{\partial u_1}{\partial x_2}\right)^2 = -\frac{\partial p}{\partial x_2} + 2(2\alpha_1 + \alpha_2)\frac{\partial u_1}{\partial x_2}\frac{\partial^2 u_1}{\partial x_2^2}$$

$$\nabla \cdot \boldsymbol{\sigma}|_z = -\frac{\partial p}{\partial x_3}.$$

Writing $\lambda = (2\alpha_1 + \alpha_2)$, $x_1 = x, x_2 = y, x_3 = z$ and $u_1 = u, u_2 = v, u_3 = w$, we have the momentum equation as

$$u\frac{\partial u}{\partial x} + v\frac{\partial u}{\partial y} + w\frac{\partial u}{\partial z} = -\frac{1}{\rho}\frac{\partial p}{\partial x} + \frac{\mu}{\rho}\frac{\partial^2 u}{\partial y^2} \tag{2.9}$$

$$u\frac{\partial v}{\partial x} + v\frac{\partial v}{\partial y} + w\frac{\partial v}{\partial z} = -\frac{1}{\rho}\frac{\partial p}{\partial y} + \lambda\frac{\partial u}{\partial y}\frac{\partial^2 u}{\partial y^2} \tag{2.10}$$

$$u\frac{\partial w}{\partial x} + v\frac{\partial w}{\partial y} + w\frac{\partial w}{\partial z} = -\frac{1}{\rho}\frac{\partial p}{\partial z} \tag{2.11}$$

The flow under consideration is such that the walls are stationary and not stretching/shrinking and aligning with the no-slip condition, the accompanying boundary conditions at the walls are;

$$u(\pm h) = 0.$$

Figure (2..1) clearly shows velocity attains maximum when $y = 0$, hence, the other boundary condition is

$$\left.\frac{\partial u}{\partial y}\right|_{y=0} = 0.$$

Thus, the equations governing the flow are

$$\frac{\partial u}{\partial x} + \frac{\partial v}{\partial y} + \frac{\partial w}{\partial z} = 0 \tag{2.12}$$

$$u\frac{\partial u}{\partial x}+v\frac{\partial u}{\partial y}+w\frac{\partial u}{\partial z}=-\frac{1}{\rho}\frac{\partial p}{\partial x}+\frac{\mu}{\rho}\frac{\partial^2 u}{\partial y^2} \tag{2.13}$$

$$u\frac{\partial v}{\partial x}+v\frac{\partial v}{\partial y}+w\frac{\partial v}{\partial z}=-\frac{1}{\rho}\frac{\partial p}{\partial y}+\lambda\frac{\partial u}{\partial y}\frac{\partial^2 u}{\partial y^2} \tag{2.14}$$

$$u\frac{\partial w}{\partial x}+v\frac{\partial w}{\partial y}+w\frac{\partial w}{\partial z}=-\frac{1}{\rho}\frac{\partial p}{\partial z} \tag{2.15}$$

with the boundary and initial conditions

$$\text{at}\ \ y=\pm h;\ \ u=0. \tag{2.16}$$

$$\text{at}\ \ y=0;\ \ \frac{\partial u}{\partial y}=0 \tag{2.17}$$

3. Analytical Solution

The analytical solution to the governing equations will be sought in three stages (Oke, 2017). The first stage is the use of substitution of the flow assumptions, the second stage involves the use of techniques for solving ordinary differential equations. Starting by substituting conditions (2.6) and (2.7) in the momentum equation (2.13) gives

$$u(0)+(0)\frac{\partial u}{\partial y}+(0)(0)=-\frac{1}{\rho}\frac{\partial p}{\partial x}+\frac{\mu}{\rho}\frac{\partial^2 u}{\partial y^2}$$

$$0=-\frac{1}{\rho}\frac{\partial p}{\partial x}+\frac{\mu}{\rho}\frac{\partial^2 u}{\partial y^2},$$

$$\mu\frac{\partial^2 u}{\partial y^2}=\frac{\partial p}{\partial x}. \tag{3.1}$$

Observe also that by conditions (2.6) and (2.7), the following holds;

$$\frac{\partial v}{\partial x}=\frac{\partial v}{\partial y}=\frac{\partial v}{\partial z}=\frac{\partial w}{\partial x}=\frac{\partial w}{\partial y}=\frac{\partial w}{\partial z}=0,$$

$$\frac{\partial^2 v}{\partial x^2}=\frac{\partial^2 v}{\partial y^2}=\frac{\partial^2 v}{\partial z^2}=\frac{\partial^2 w}{\partial x^2}=\frac{\partial^2 w}{\partial y^2}=\frac{\partial^2 w}{\partial z^2}=0.$$

Using the above results in the other momentum equations (2.14) and (2.15), we have

$$u(0)+(0)(0)+(0)(0)=-\frac{1}{\rho}\frac{\partial p}{\partial y}+\lambda\frac{\partial u}{\partial y}\frac{\partial^2 u}{\partial y^2}\ \ \Rightarrow\ \ \lambda\frac{\partial u}{\partial y}\frac{\partial^2 u}{\partial y^2}=\frac{1}{\rho}\frac{\partial p}{\partial y} \tag{3.2}$$

$$u(0)+(0)(0)+(0)(0)=-\frac{1}{\rho}\frac{\partial p}{\partial z}+\frac{\mu}{\rho}\big((0)+(0)+(0)\big)\ \ \Rightarrow\ \ \frac{\partial p}{\partial z}=0 \tag{3.3}$$

The independence of u on the z-direction and the condition (2.8), then $u=u(y)$. Also, equation (3.3) implies that pressure does not change in the z-direction. Based on these, equation (3.1) can be re-arranged as;

$$\mu\frac{d^2 u}{dy^2}=\frac{\partial p}{\partial x}\ \ \Rightarrow\ \ \frac{d^2 u}{dy^2}=\frac{1}{\mu}\frac{\partial p}{\partial x}. \tag{3.4}$$

Substitute equation (3.4) into equation (3.2), we get

$$\lambda\frac{du}{dy}\frac{d^2 u}{dy^2}=\frac{1}{\rho}\frac{\partial p}{\partial y}\quad\Rightarrow\lambda\frac{du}{dy}\left(\frac{1}{\mu}\frac{\partial p}{\partial x}\right)=\frac{1}{\rho}\frac{\partial p}{\partial y}$$

$$\Rightarrow\lambda\frac{du}{dy}=\frac{\mu}{\rho}\left(\frac{\partial p}{\partial y}\div\frac{\partial p}{\partial x}\right)$$

$$\Rightarrow\int\lambda\frac{du}{dy}dy=\int\frac{\mu}{\rho}\left(\frac{\partial p}{\partial y}\div\frac{\partial p}{\partial x}\right)dy$$

$$\Rightarrow\quad\lambda u=\frac{\mu}{\rho}\int\left(\frac{\partial p}{\partial y}\div\frac{\partial p}{\partial x}\right)dy+c.$$

Consider a pressure distribution of the form

$$p(x,y)=x^2+y^2, \tag{3.5}$$

we have

$$\frac{\partial p}{\partial x}=2x,\qquad\frac{\partial p}{\partial y}=2y.$$

Thus,

$$\lambda u = \frac{\mu}{\rho}\int \frac{y}{x}dy + c \;\Rightarrow\; \lambda u = \frac{\mu y^2}{2\rho x} + c.$$

Using the boundary condition

$$u = 0, \text{ when } y = \pm h,$$

we have

$$\lambda(0) = \frac{\mu h^2}{2\rho x} + c \;\Rightarrow\; c = -\frac{\mu h^2}{2\rho x}.$$

Finally, we have

$$\lambda u = \frac{\mu y^2}{2\rho x} - \frac{\mu h^2}{2\rho x} = \frac{\mu}{2\rho x}(y^2 - h^2). \tag{3.6}$$

Now since on differentiation, we have

$$\lambda\frac{du}{dy} = \frac{\mu y}{\rho x} \;\Rightarrow\; \frac{du}{dy} = 0, \text{ when } y = 0,$$

then the second condition is automatically satisfied. The solution is therefore

$$u = \frac{\mu}{2\lambda\rho x}(y^2 - h^2).$$

3.1 Numerical simulation

Considering blood as a second-grade fluid, we take the default values as $h = 1.5m$, $\rho = 1050kgm^{-3}$, and $\mu = 3.5$ and $\lambda = 2m^2$. To verify the shape of the velocity profile, we plot the graph of u when $x = 0.15m$ and the graph is displayed in Figure 2. The parabola nature of the graph indicates that flow is Poiseuille, just as expected.

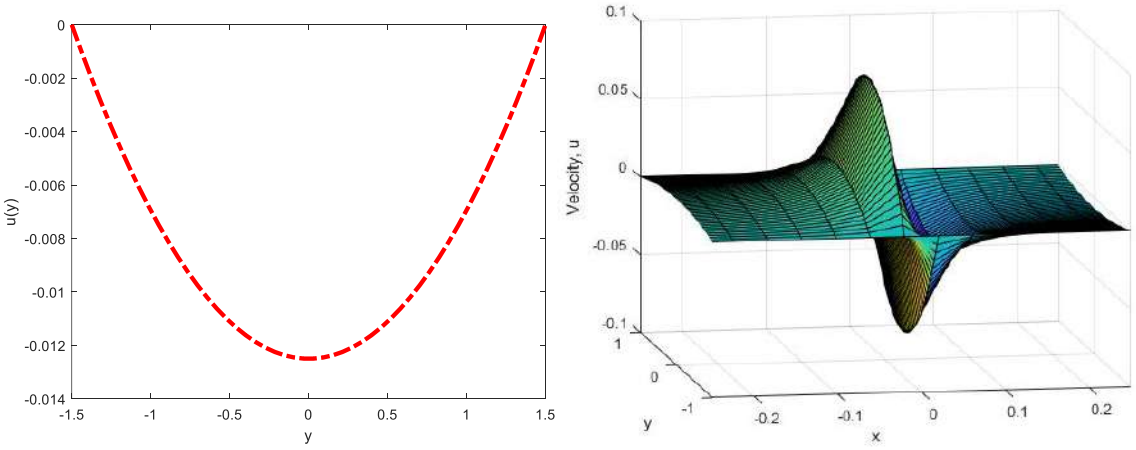

Figure 2: Showing velocity profile for Poiseuille flow

The flow rate for the second-grade fluid is denoted as Q and defined as:

$$Q = \int_{-h}^{h} u dy$$

so,

$$Q = \int_{-h}^{h} u dy = \int_{-h}^{h} \frac{\mu}{2\lambda\rho x}(y^2 - h^2)dy = \frac{\mu}{2\lambda\rho x}\int_{-h}^{h}(y^2 - h^2)dy = \frac{\mu}{2\lambda\rho x}\left[\frac{y^3}{3} - yh^2\right]_{-h}^{h}$$

$$= \frac{\mu}{2\lambda\rho x}\left[\left(\frac{h^3}{3} - h^3\right) - \left(\frac{-h^3}{3} - h^3\right)\right] = \frac{\mu h^3}{3\lambda\rho x}.$$

It can be seen from Figure 3 that the flow rate attains maximum at the highest value of h.

$$h = 1.5m;\;\; \rho = 1050;\;\; \mu = 3.5;\;\; \lambda = 2.$$

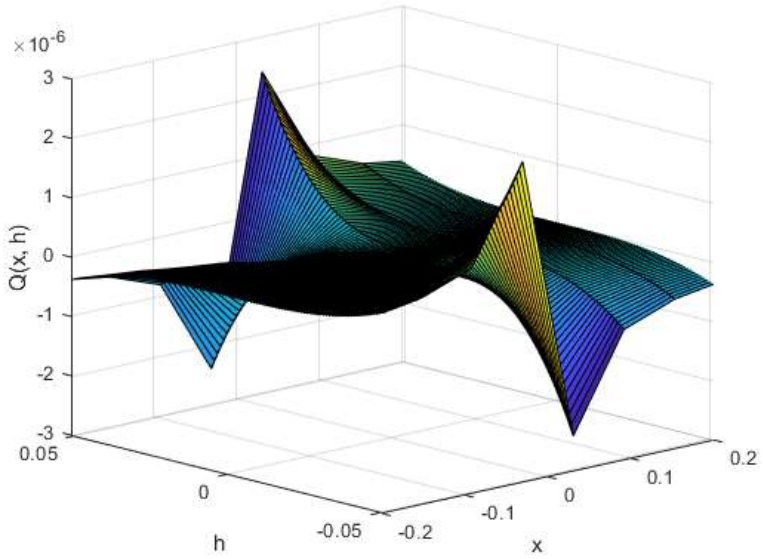

Figure 3: Flow rate

4. Analysis and Discussion of Results

The analytical results obtained in section 3 for velocity and flow rate are plotted against the distance y at varying values of the flow parameters to identify the behaviour of second-grade Poiseuille flow. The responses of velocity and flow rate to the variation in the flow parameters are discussed as follows. Figure 4 shows the behaviour of velocity distribution in the flow as the pipe radius increases. The velocity distribution reduces as the pipe radius increases as displayed in Figure 4. According to the continuity principle, the mass flow rate is constant throughout the pipe. Hence, with an increasing pipe radius, the velocity reduces to obey the law of mass conservation. Figure 5 shows the velocity profile as the fluid becomes fully second-grade. When $\lambda = 0$, the fluid becomes Newtonian while the fluid becomes purely second-grade as λ increases. The velocity profile shown in Figure 5 indicates a decrease in velocity as the fluid becomes purely second-grade. The visco-elasticity nature of the second-grade fluid contributes to the increase in the boundary layer thickness, thereby causing more drag near the wall of the pipe and consequently leading to an overall reduction in the flow velocity. The flow rate is also found to decrease with increasing material parameter λ. Figure 6 shows the decrease in the flow rate as the material parameter increases. Figure 7 is a representation of the behaviour of velocity as the dynamic viscosity increases. It can be seen that velocity increases as the viscosity increases while the flow rate decreases as the material parameter increases (see Figure 8). Figure 9 shows the velocity distribution at different cross-sectional areas of the pipe. The flow velocity reduces as the flow progresses further into the pipe as shown in Figure 9.

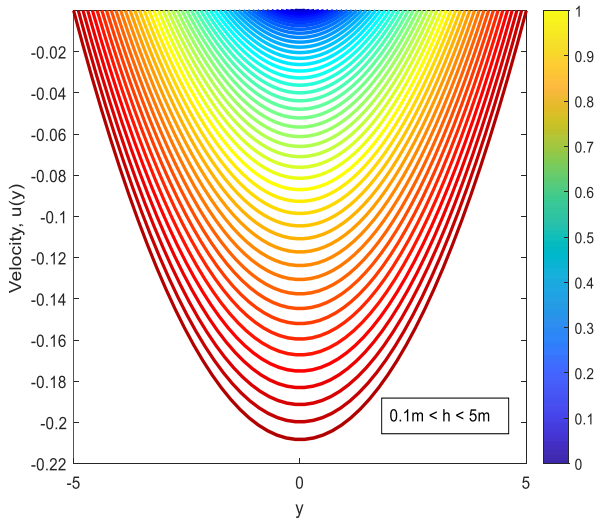

Figure 4: Velocity profile for various values of pipe

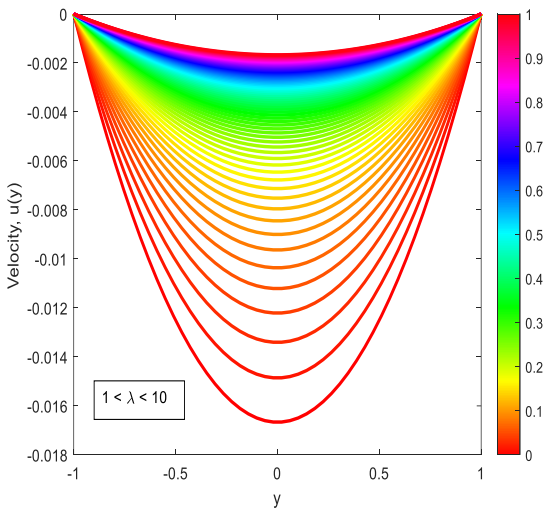

Figure 5: Velocity profile for various values of

radius

material parameter

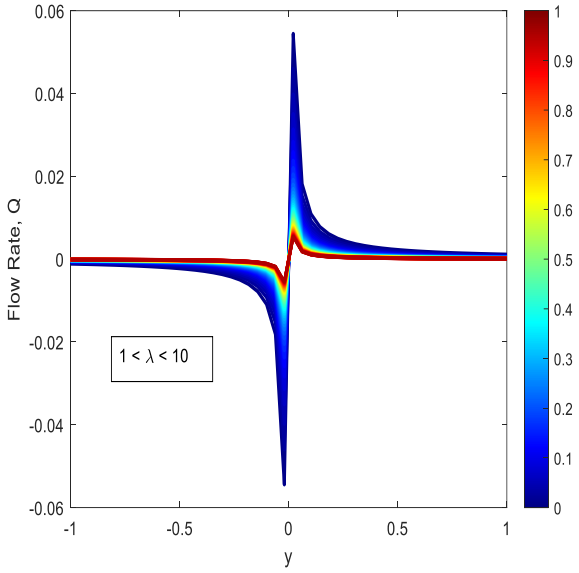

Figure 6: Flow rate for various values of material parameter

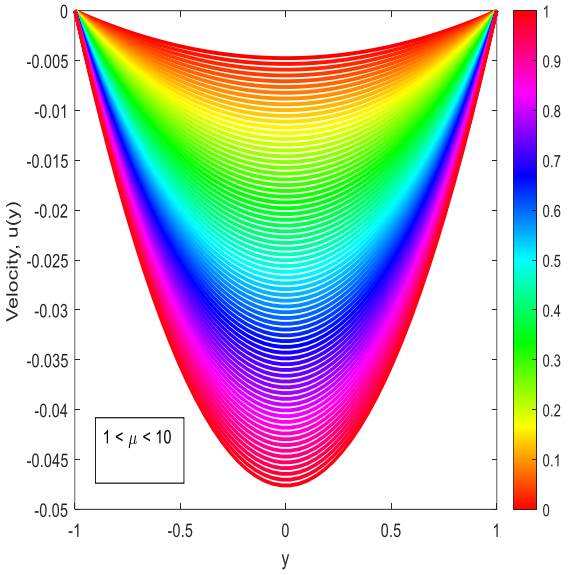

Figure 7: Velocity profile for various values of viscosity

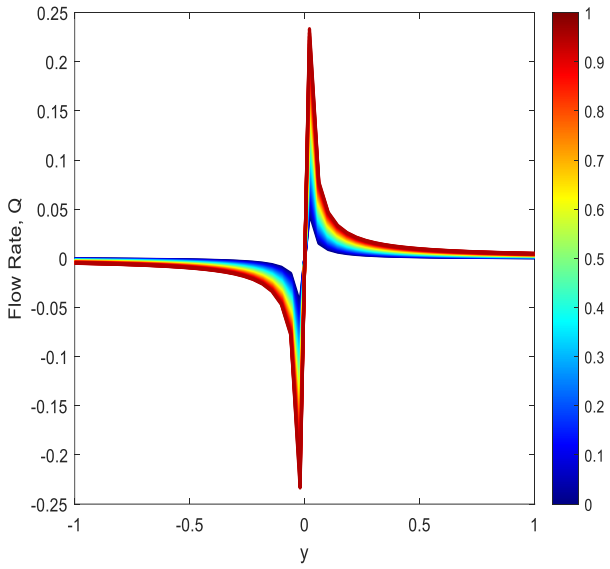

Figure 8: Flow rate for various values of viscosity

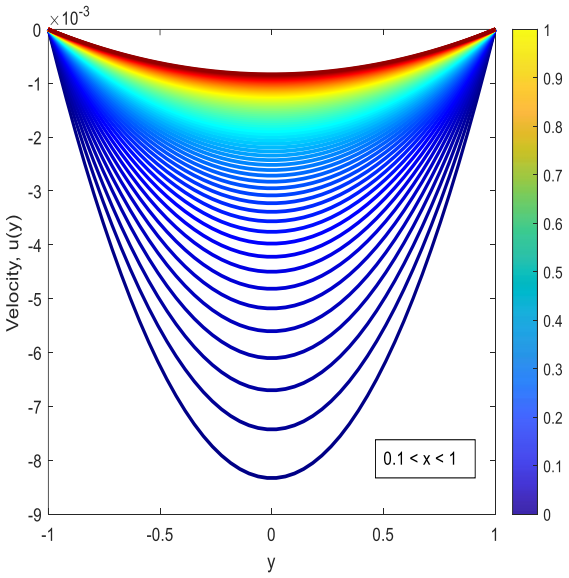

Figure 9: Velocity profile at different cross-sections of the flow

5. Conclusion

The flow of second-grade fluid in a non-moving non-stretching plates is investigated in this study. The equations governing the flow were derived from and the analytical solution to the flow was found. The velocity distribution shows the parabola shape indicating the flow is Poiseuille flow. The results show that;

- The velocity distribution reduces as the pipe radius increases.
- The velocity profile decreases as the fluid becomes purely second-grade.
- flow rate is also found to decrease with increasing material parameter λ.

- velocity increases as the viscosity increases
- flow rate decreases as the material parameter increases.

References

Andersson, H. I. (1992). MHD flow of a viscoelastic fluid past a stretching surface. Acta Mechanica, 95(1-4), 227-230. https://doi.org/10.1007/BF01170814
Ayub, M. & Zaman, H. (2010). Complete derivation of the momentum equation for the second-grade fluid. Journal of Mathematics and Computer Science, 1(1), 33-39. https://doi.org/10.22436/jmcs.001.01.05
Beard, D. W. (1964). Elastico-viscous boundary-layer flows i. two-dimensional flow near a stagnation point. . Mathematical Proceedings of the Cambridge Philosophical Society, 60(3), 667-674. https://doi.org/10.1017/S0305004100038147
Coles, D., 1965. Transition in circular Couette flow. Journal of Fluid Mechanics, 21(3), pp.385-425. https://doi.org/10.1017/S0022112065000241
Divya, G. P., Reddy, G. V., & Bindu, P. (2023, May). Unsteady MHD Casson and Williamson nanofluids over a permeable stretching sheet in the presence of thermal radiation and chemical reaction. In AIP Conference Proceedings (Vol. 2707, No. 1). AIP Publishing. https://doi.org/10.1063/5.0143359
Gee, B. and Gracie, R., 2022. Beyond Poiseuille flow: A transient energy-conserving model for flow through fractures of varying aperture. Advances in Water Resources, 164, p.104192. https://doi.org/10.1016/j.advwatres.2022.104192
Juma, B. A., Oke, A. S., Mutuku, W. N., Ariwayo, A. G., & Ouru, O. J. (2022). Dynamics of Williamson fluid over an inclined surface subject to Coriolis and Lorentz forces. Engineering and Applied Science Letter, 5(1), 37-46.
Kọríkọ, O. K., Adegbie, K. S., Oke, A. S., & Animasaun, I. L. (2020). Exploration of Coriolis force on motion of air over the upper horizontal surface of a paraboloid of revolution. Physica Scripta, 95(3), 035210. https://doi.org/10.1088/1402-4896/ab4c50
Krishna, M. V., Ahamad, N. A., & Chamkha, A. J. (2021). Hall and ion slip impacts on unsteady MHD convective rotating flow of heat generating/absorbing second grade fluid. Alexandria Engineering Journal, 60(1), 845-858. https://doi.org/10.1016/j.aej.2020.10.013
Kumar K. A. , Reddy Ramana J.V., Sugunamma V. , Sandeep N. (2018a). Magnetohydrodynamic Cattaneo-Christov flow past a cone and a wedge with variable heat source/sink. Alexandria Engineering Journal, 57(1), pp 435-443 https://doi.org/10.1016/j.aej.2016.11.013
Kumar K. A., Sugunamma V. & Sandeep N. (2018b). Impact of Non-linear Radiation on MHD Non-aligned Stagnation Point Flow of Micropolar Fluid Over a Convective Surface. Journal of Non-Equilibrium Thermodynamics, 43(4), 327-345 https://doi.org/10.1515/jnet-2018-0022
Kumar K. A., Sugunamma V., Sandeep N. (2019a). A non-Fourier heat flux model for magnetohydrodynamic micropolar liquid flow across a coagulated sheet. Heat Transfer-Asian Res. 48, pp 2819-2843 https://doi.org/10.1002/htj.21518
Kumar K. A., Sugunamma V., Sandeep N. (2020). Influence of viscous dissipation on MHD flow of micropolar fluid over a slendering stretching surface with modified heat flux model. Journal of Thermal Analysis and Calorimetry, 139, pp 3661-3674 https://doi.org/10.1007/s10973-019-08694-8
Kumar K.A., Sugunamma V., Sandeep N. (2019b) et al. Simultaneous solutions for first order and second order slips on micropolar fluid flow across a convective surface in the presence of Lorentz force and variable heat source/sink. Science Reports 9, 14706 https://doi.org/10.1038/s41598-019-51242-5
Murthy, C. V., & Reddy, G. (2023). MHD Casson and Carreau fluid flow through a porous medium with variable thermal conductivity in the presence of suction/injection. Journal of Naval Architecture & Marine Engineering, 20(1).
Oke, A. S. (2017). Convergence of differential transform method for ordinary differential equations. Journal of Advances in Mathematics and Computer Science, 24(6), 1-17. https://doi.org/10.9734/JAMCS/2017/36489
Oke, A. S. (2021). Coriolis effects on MHD flow of MEP fluid over a non-uniform surface in the presence of thermal radiation. International Communications in Heat and Mass Transfer, 129, 105695. https://doi.org/10.1016/j.icheatmasstransfer.2021.105695
Oke, A. S. (2022). Theoretical analysis of modified eyring powell fluid flow. Journal of the Taiwan Institute of Chemical Engineers, 132, 104152. https://doi.org/10.1016/j.jtice.2021.11.019

Oke, A. S. (2022b). Heat and mass transfer in 3D MHD flow of EG-based ternary hybrid nanofluid over a rotating surface. Arabian Journal for Science and Engineering, 47(12), 16015-16031. https://doi.org/10.1007/s13369-022-06838-x

Oke, A. S. (2022c). Combined effects of Coriolis force and nanoparticle properties on the dynamics of gold-water nanofluid across nonuniform surface. ZAMM-Journal of Applied Mathematics and Mechanics/Zeitschrift für Angewandte Mathematik und Mechanik, 102(9), e202100113. https://doi.org/10.1002/zamm.202100113

Oke, A. S., Animasaun, I. L., Mutuku, W. N., Kimathi, M., Shah, N. A., & Saleem, S. (2021). Significance of Coriolis force, volume fraction, and heat source/sink on the dynamics of water conveying 47 nm alumina nanoparticles over a uniform surface. Chinese Journal of Physics, 71, 716-727. https://doi.org/10.1016/j.cjph.2021.02.005

Oke, A.S., Eyinla, T. and Juma, B.A., 2023. Effect of Coriolis force on modified eyring powell fluid flow. Journal of Engineering Research and Reports, 24(4), pp.26-34. https://doi.org/10.9734/jerr/2023/v24i4811

Oke, A.S., Mutuku, W.N., Kimathi, M. and Animasaun, I.L., 2020. Insight into the dynamics of non-Newtonian Casson fluid over a rotating non-uniform surface subject to Coriolis force. Nonlinear Engineering, 9(1), pp.398-411. https://doi.org/10.1515/nleng-2020-0025

Rani, K. S., Reddy, G. V. R., & Oke, A. S. (2023). Significance of Cattaneo-Christov heat flux on chemically reacting nanofluids flow past a stretching sheet with joule heating effect. CFD Letters, 15(7), 31-41. https://doi.org/10.37934/cfdl.15.7.3141

Reddy, K. V., & Reddy, G. V. R. (2022). Outlining the impact of melting on MHD Casson fluid flow past a stretching sheet in a porous medium with radiation. Biointerface Research in Applied Chemistry, 13, 1-14. https://doi.org/10.33263/BRIAC131.042

Sitamahalakshmi, V., Reddy, G. V. R., & Falodun, B. O. (2023). Heat and mass transfer effects on MHD Casson fluid flow of blood in stretching permeable vessel. Journal of Applied Nonlinear Dynamics, 12(01), 87-97. https://doi.org/10.5890/JAND.2023.03.006

Sulaimon, A.A., Sannang, M.Z., Nazar, M. and Shariff, A.M., 2023. Investigating the effect of okra mucilage on waxy oil flow in pipeline. Journal of Advanced Research in Fluid Mechanics and Thermal Sciences, 107(2), pp.41-49. https://doi.org/10.37934/arfmts.107.2.4149

Tharapatla, G., RajKumari, P., & Ramana Reddy, G. V. (2021). Effects of heat and mass transfer on MHD nonlinear free convection non-Newtonian fluids flow embedded in a thermally stratified porous medium. Heat Transfer, 50(4), 3480-3500. https://doi.org/10.1002/htj.22037

Vyakaranam, S. V., Pathuri, B., Gurrampati, V. R. R., & Oke, A. S. (2022). Flow of Casson nanofluid past a permeable surface: effects of Brownian motion, thermophoretic diffusion and Lorenz force. CFD Letters, 14(12), 111125-111125. https://doi.org/10.37934/cfdl.14.12.111125

Wu, S., Xu, Z., Jian, R., Tian, S., Zhou, L., Luo, T. and Xiong, G., 2023. Molecular alignment-mediated stick-slip poiseuille flow of oil in graphene nanochannels. The Journal of Physical Chemistry B, 127(27), pp.6184-6190. https://doi.org/10.1021/acs.jpcb.3c01805

Yavuz, M., Sene, N., & Yıldız, M. (2022). Analysis of the influences of parameters in the fractional second-grade fluid dynamics. Mathematics, 10(7), 1125. https://doi.org/10.3390/math10071125